Title

NaI revisited: Theoretical investigation of predissociation via ultrafast XUV transient absorption spectroscopy.

Journal

The Journal of chemical physics, 151(20)

ISSN

0021-9606

Authors

Kobayashi, Yuki
Zeng, Tao
Neumark, Daniel M
et al.

Publication Date

2019-11-01

DOI

10.1063/1.5128105

Peer reviewed

NaI revisited: theoretical investigation of predissociation via ultrafast XUV transient absorption spectroscopy

Yuki Kobayashi,[1, a)] Tao Zeng,[2] Daniel M. Neumark,[1, 3] and Stephen R. Leone[1, 3, 4]
[1)] *Department of Chemistry, University of California, Berkeley, California 94720, USA*
[2)] *Department of Chemistry, York University, Toronto, Ontario M3J1P3, Canada*
[3)] *Chemical Sciences Division, Lawrence Berkeley National Laboratory, Berkeley, California 94720, USA*
[4)] *Department of Physics, University of California, Berkeley, California 94720, USA*

(Dated: 12 September 2019)

Avoided crossings can trigger abrupt changes of electronic character and redirect the outcomes of photochemical reactions. Here, we report a theoretical investigation into core-level spectroscopic probing of predissociation dynamics of sodium iodide (NaI), a prototype system for studies of avoided-crossing dynamics. The elegant femtochemistry work of Zewail and co-workers pioneered the real-time dynamics of NaI, detecting the Na atoms bursting forth from the avoided crossing and the residual NaI molecules oscillating inside the quasi-bound potential. The simulated results show that core-level spectroscopy not only observes these integrated outcomes, but also provides a direct measure of the abrupt switching of electronic character at the avoided crossing. The valence and core-excited electronic structures of NaI are computed by spin-orbit general multi-configurational quasi-degenerate perturbation theory, from which core-level absorption spectra of the predissociation dynamics are constructed. The wave-packet motion on the covalent potential is continuously mapped as shifts in the absorption energies, and the switching between the covalent and ionic character at the avoided crossing is characterized as the sharp rise and fall of the Na^+ signal. The Na^+ signal is found to be insensitive to the wave-packet motion in the asymptotic part of the ionic potential, which in turn enables a direct measure of the nonadiabatic crossing probability excluding the effect of wave-packet broadening.

I. INTRODUCTION

The progress in ultrafast laser technology in the 1980s led to the invention of femtosecond transient-state spectroscopy (FTS).[1,2] The new spectroscopic method realized the first time-resolved measurements of elementary chemical reactions that occur on femtosecond time scales such as photodissociation[3] and predissociation.[4,5] Today, attosecond light sources in the extreme-ultraviolet (XUV) to x-ray regimes produced through the process of high-harmonic generation are available as a new tool for ultrafast spectroscopy.[6,7] Attosecond spectroscopy was initiated in the field of atomic physics, and an increasing number of applications are reported in the exploration of chemical dynamics.[8–12] With the unprecedented time resolution and the unique accessibility to atom-specific core orbitals, attosecond spectroscopy represents a powerful new way to address molecular dynamics, revitalizing interest in revisiting classical problems of chemical physics.[13]

Of particular importance is the ability to directly probe avoided crossings and conical intersections, where two or more reaction potentials come to degeneracy (or pseudo-degeneracy) and start to couple nonadiabatically.[14,15] The coupling can induce photoexcited molecules to undergo nonadiabatic population transfer or rapidly switch their electronic character between the coupled states.[16–20] Those elusive processes have been a subject of numerous spectroscopic studies for their ubiquitous role in steering the outcome of photochemical reactions.[15,21–34] Despite the established concept of potential crossings, their experimental observation is still considered challenging, as it requires few-femtosecond time resolution and a capability to resolve closely-spaced electronic states by the probe method.

Here, we theoretically investigate the application of ultrafast XUV transient absorption spectroscopy to the classic curve-crossing dynamics of sodium iodide (NaI). Sodium iodide has served as a prototype for curve-crossing problems; the pioneering FTS experiments of Zewail and co-workers successfully resolved the quasi-bound motion of the photoexcited molecule[4,5], and several follow-up studies were conducted experimentally and theoretically.[35–50] In those seminal studies, the wave-packet motion inside and outside of the crossing region were observed, with bursts of Na atoms leaking out via the crossing and the diminishing NaI molecules inside the crossing region. Our results show the capability of ultrafast XUV transient absorption spectroscopy to resolve not only the quasi-bound motion of the photoexcited molecule, but also the rapid switching of electronic character at the avoided crossing, the key process induced by state coupling.

The use of ultrafast XUV pulses in the transient-absorption configuration is advantageous in that both a wide spectral coverage and ultimate attosecond time

[a)] Electronic mail: ykoba@berkeley.edu

resolution can be achieved simultaneously[51]. Furthermore, core-level absorption is sensitive to subtle changes in valence electronic states, and one can retrieve detailed information on the target molecules such as the bond lengths, charge states, and spin-orbit fine structure. In terms of a typical probing scheme, NaI is an ideal target since both the Na and I atoms have characteristic core-level resonances within the spectral coverage of the attosecond XUV pulse[52]; ~ 35 eV for Na-2p orbitals, and ~ 50 eV for the I-4d orbitals.

First we review the predissociative potentials of NaI (Fig. 1).[53] The alphabetical letters X, A, and B are used to indicate the energy order for the states with $\Omega = 0^+$, where Ω is the projection of the total angular momentum along the Na-I axis. The other potentials with $\Omega = 0^-, 1, 2$ do not participate in the excited-state dynamics and their potentials are hence not shown here. The ground X(0^+) state corresponds to the $[\sigma^2\pi^4\sigma^{*0}]$ configuration and it has ionic character in the Franck-Condon region. Ultraviolet photoexcitation promotes the molecule to the covalent A(0^+) state, which arises from the $[\sigma^1\pi^4\sigma^{*1}]$ configuration. The ionic and covalent potentials come to near degeneracy at the internuclear distance of $R \sim 7$ Å, at which an avoided crossing of intermediate strength occurs. There are two possible pathways at the avoided crossing (Fig. 1, gray arrows). One is the diabatic pathway, in which the photoexcited molecule conserves the covalent character and dissociates toward the Na($^2S_{1/2}$) + I($^2P_{3/2}$) asymptote. The other is the adiabatic pathway, in which the photoexcited molecule transfers to the ionic potential and gets trapped by the attractive Coulomb potential. The excited B(0^+) state is well separated in energy from the A(0^+) potential by ~ 1 eV corresponding to the spin-orbit splitting of the I(^2P) states, and the contribution of the B(0^+) state is negligible to the predissociation dynamics of interest.

The strength of the avoided crossing bears mentioning. In previous work[4,5], a substantial ($\sim 10\%$) dissociation probability per crossing was estimated. In the calculations here, much of this experimentally estimated probability may come from wave packet broadening, while the actual calculated dissociation probability per crossing is less, around 1%. This does not change the dynamical features throughout the discussion, and even minor channels are accounted for in detail in Appendix.

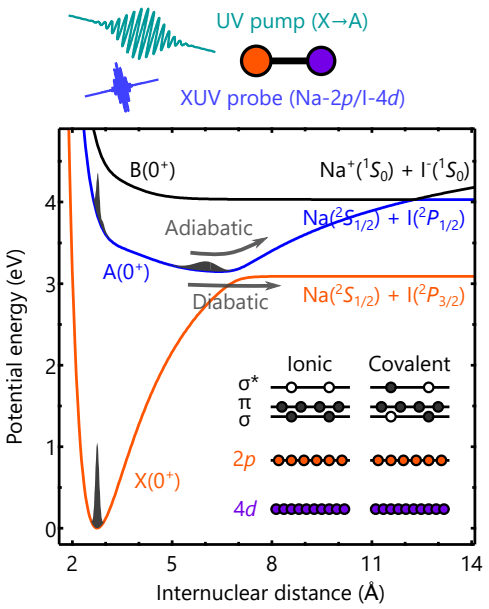

FIG. 1. **Predissociative potentials of NaI.** The top panel shows the pump-probe scheme of the present simulation, and the lower panel shows the computed adiabatic potentials of NaI. The ground X(0^+) state is of ionic character and corresponds to the $[\sigma^2\pi^4\sigma^{*0}]$ configuration. Ultraviolet photoexcitation promotes the molecule to the excited A(0^+) state, which is of covalent character and belongs to the $[\sigma^1\pi^4\sigma^{*1}]$ configuration. At the avoided crossing at ~ 7 Å, the photoexcited molecule will either diabatically evolve to the dissociation asymptote, or adiabatically transfer to the bound ionic potential. Snapshots of the nuclear wave packets are shown as gray areas corresponding to $t = -200$ fs on the X(0^+) potential, and $t = 0$ fs and 150 fs on the A(0^+) potential. The labels for the product states are denoted such that their colors match the corresponding potentials in the asymptote.

II. METHODS

A. Electronic-structure calculations

The electronic structure of NaI is computed by using spin-orbit general multi-configurational quasi-degenerate perturbation theory (SO-GMC-QDPT) implemented in the developer version of GAMESS-US[54]. The SO-GMC-QDPT method is able to include all the key factors for the computation of halogen-containing molecules, i.e., static and dynamic correlations as well as spin-orbit coupling.[55–59] Flexible setting of active spaces available through the occupation-restricted multiple active space scheme (ORMAS) facilitates the computation of core-excited states.[55–57]

In all calculations, model-core potentials and basis sets of triple-zeta quality (MCP-TZP)[60,61] are used. A Hartree-Fock calculation is performed at the ground-state equilibrium distance ($R = 2.71$ Å),[62] and the resultant molecular orbitals are used as an initial input for the subsequent GMC-QDPT calculations. Two active spaces are defined based on the ORMAS scheme.[55–57] A valence-active space consists of the Na-3s and I-5p orbitals containing 6 electrons in 4 orbitals. A core-active space consists of the Na-2p and I-4d orbitals containing 16 electrons in 8 orbitals. The valence-active space is taken as a complete active space, i.e., the 6 valence electrons are freely distributed in the 4 valence orbitals. From the core-active space, single excitations into the valence-active space are allowed, which mimic the core-to-valence excitations by the XUV probe pulse. The spin-free GMC-QDPT states are used as multi-electron basis

states to calculate spin-orbit matrix elements, which are then diagonalized to yield the final spin-orbit perturbed electronic states.

In order to accurately account for the spin-orbit couplings in the relevant electronic shells (i.e., I-4d, I-5p, and Na-2p), we adjusted three empirical parameters as follows. Effective nuclear charges of $Z_{\text{eff}} = 65.22$ and 9.19 are used for the I and Na atomic nuclei, respectively, to reproduce the spin-orbit splittings in the I-5p and Na-2p shells. Additionally, the spin-orbit coupling constant of the I-4d shell is scaled down by a factor of 0.632 to reproduce the spin-orbit splitting of the I-4d shell. The spin-orbit splittings of the I-4d and I-5p shells are referenced from O'Sullivan et al. (1.70 eV and 0.94 eV, respectively),[63] and that for the Na-2p orbital is from Wolff et al. (0.17 eV).[64] Constant energy shifts of +0.07 eV and −2.21 eV are added to the I-4d and Na-2p core-excited potentials, respectively, to reproduce the I $4d \rightarrow 5p$ and Na $2p \rightarrow 3s$ atomic core-to-valence transitions.[63,64] These manual settings are necessary because the basis sets are optimized only for the energy of the atomic ground state, not to accurately reproduce the experimental XUV spectra.[59] A recent experimental work confirmed the SO-GMC-QDPT results can reproduce the core-level absorption spectra throughout the reaction coordinates with these manual settings.[15]

Spectroscopic parameters of the valence potentials are analyzed to evaluate the accuracy of the calculation results. For the ground $X(0^+)$ state, the equilibrium internuclear distance and harmonic frequency are calculated to be 2.75 Å and 250.9 cm^{-1}, respectively, which compare well with the experimental values of 2.71 Å and 259.2 cm^{-1}.[62] The location of the avoided crossing is computed to be at 7.01 Å, where the energy separation minimizes to be 0.135 eV. These values also compare well with other recent calculations (6.8 Å and 0.153 eV).[50] The equilibrium bond length of the $A(0^+)$ state is computed to be 6.39 Å. The present value compares relatively well with the latest calculation (6.260 Å),[50] but it is somewhat larger than the experimental estimate (6.052 Å).[65] Note that the shape of the $A(0^+)$ potential remains a topic of debate, as it is highly affected by coupling with the $X(0^+)$ state.[36,50,65] Overall, we conclude that the calculated potentials provide a qualitatively correct description of the predissociation dynamics. The results could be improved by including the Na-3p orbitals into calculations, but such expansion of the active space is computationally too demanding for the present core-level calculations.

B. Nuclear wave packet simulations

The predissociation dynamics are simulated by numerically solving the time-dependent Schrödinger equation. The Hamiltonian of the diatomic system including the nonadiabatic couplings and laser-dipole interactions takes the form,[66]

$$\boldsymbol{H}(R,t) = \left[-\frac{1}{2m}\frac{\partial^2}{\partial R^2} + \boldsymbol{V}(R) + \boldsymbol{\mu}(R)E(t)\right] + \left[-\frac{1}{m}\boldsymbol{D}_1(R)\frac{\partial}{\partial R} - \frac{1}{2m}\boldsymbol{D}_2(R)\right]. \quad (1)$$

In Equation (1), R is the internuclear distance, m is the reduced mass of the molecule, $\boldsymbol{V}$ is the adiabatic potentials, $\boldsymbol{\mu}$ is the transition dipole, and E is the laser electric field of the ultraviolet (UV) excitation pulse. The last two terms in the second bracket represent the nonadiabatic interactions, in which the matrices $\boldsymbol{D}_1$ and $\boldsymbol{D}_2$ are the first-order and second-order nonadiabatic coupling terms.

Potential energies were first computed by SO-GMC-QDPT from 1.60 Å to 15.00 Å at intervals of 0.04 Å. The grid points were evaluated by cubic-spline interpolation and a finer grid space with intervals of 0.01 Å was obtained. The nuclear wave packets were expressed by sinc-DVR,[67] and the time propagation was performed at time intervals of 25 as by using the short-iterative Arnoldi method.[68] The initial wave packet was taken as a ground vibrational state of the $X(0^+)$ potential. The UV pump pulse was defined to have a center wavelength of 320 nm and a pulse duration (FWHM) of 20 fs. The wave packet moving toward the dissociation asymptote was smoothly removed by a complex absorbing potential to prevent the artificial reflection at the boundary.[69]

III. RESULTS AND DISCUSSION

In this section, we first examine the qualitative features of the potentials, then inspect the core-to-valence absorption strengths, and lastly simulate and analyze the core-level absorption spectra of the predissociation dynamics.

A. Overview of the potentials

An overview of the valence and core-excited potentials of NaI is shown in Fig. 2. The valence electronic states (black curves) comprise the ionic (Na^+/I^-), covalent (Na/I), and counter-ionic (Na^-/I^+) potentials. The ionic and covalent potentials are close in energy, and avoided crossings occur in the asymptotic regions (Fig. 2, gray circle). The counter-ionic states are located ~ 10 eV higher than the ionic and covalent potentials, and they are isolated from the predissociation dynamics of interest.

The Na-2p core-excited states (orange curves) are located ~ 35 eV higher than the valence states. In this state manifold, ionic and covalent potentials are present, but those that correlate with the counter-ionic asymptote are absent. This is rationalized by the fact that the valence Na-3s shell is fully occupied after the $2p \rightarrow 3s$

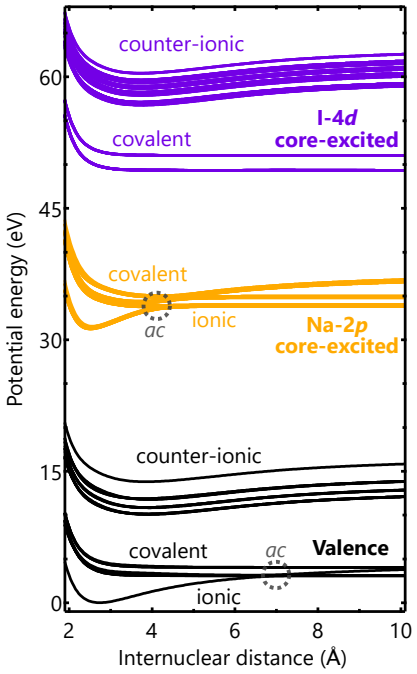

FIG. 2. **Overview of the valence and core-excited potentials.** The black, orange, and purple curves correspond to the valence, Na-2p core-excited, and I-4d core-excited electronic states, respectively. The classifications of the covalent (Na/I), ionic (Na^+/I^-), and counter-ionic (Na^-/I^+) states are denoted. The avoided crossings (ac) between the ionic and covalent potentials that are mentioned in the main text are marked by gray circles.

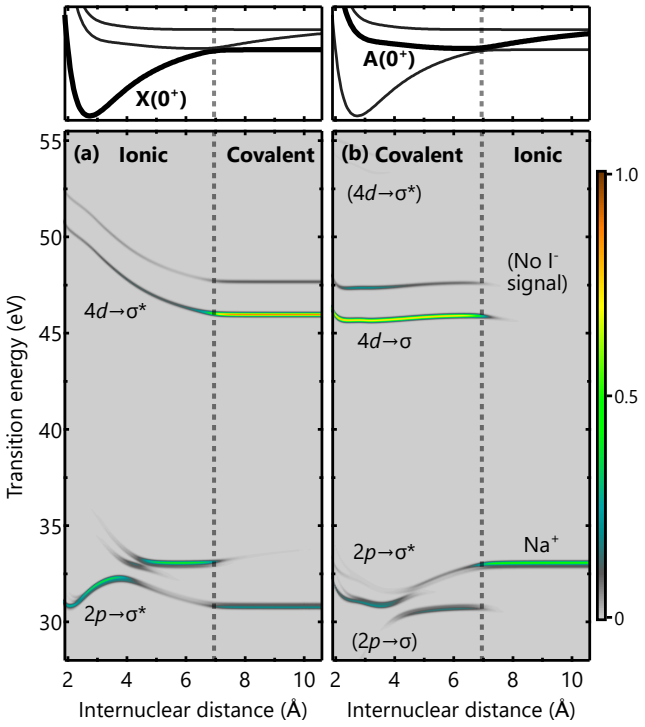

FIG. 3. **Core-to-valence absorption strengths versus internuclear distance.** Core-to-valence absorption strengths from the (a) $X(0^+)$ and (b) $A(0^+)$ states. The corresponding potential energy curves are displayed in the top panels by thick black curves. The vertical dashed line indicates the location of the avoided crossing.

core-to-valence excitation, and the doubly occupied Na-3s shell cannot accommodate an extra electron from the iodine atom to make the system counter ionic. As is similar to the valence states, the Na-2p core-excited states exhibit avoided crossings between the ionic and covalent potentials (Fig. 2, gray circle), which cause, as will be shown later, discontinuous patterns in the core-level absorption signals.

The I-4d core-excited states (purple curves) are located $\sim$ 50 eV higher than the valence states. The potentials belong to either covalent or counter-ionic states, and the potentials that correlate with the ionic asymptote are absent. This again is a result of the fact that the $4d \rightarrow 5p$ probe excitation would fill the valence I-5p shell completely and the iodine atom becomes unable to accept an extra electron from the sodium atom. Due to the absence of the ionic configurations, the I-4d core-excited potentials are free of avoided crossings.

B. Core-to-valence absorption strengths

The computed electronic structures enable us to calculate the core-to-valence absorption strengths versus internuclear distance (no dynamics yet included). Figures 3(a,b) show the results for the valence $X(0^+)$ and $A(0^+)$ states, respectively. The panels on top show the corresponding adiabatic potentials (thick black curves). The absorption strengths are calculated by taking a sum of the core-to-valence oscillator strengths convoluted with a 150-meV Gaussian broadening, which accounts for the finite autoionization lifetime of the core-excited states[63].

The Franck-Condon region of the ground $X(0^+)$ state (Fig. 3(a)), which is of ionic character, is probed by the Na 2p/I 4d $\rightarrow \sigma^*$ transitions. The doublet signals in the I-4d window correspond to the spin-orbit splitting between the $4d_{5/2}$ and $4d_{3/2}$ levels. The σ^* orbital mostly consists of the Na-3s orbital, and it has larger spatial overlap with the Na-2p orbitals than with the I-4d orbitals. As such, the core-level absorption signals are stronger in the Na-2p window. The I 4d $\rightarrow \sigma^*$ transitions can be regarded as a charge-transfer process, which changes the character of the system from ionic to covalent. This leads to dramatic variation in the potential shape as seen in Fig. 2, from bound (ionic) to nearly flat and dissociative (covalent), which is reflected in the $4d \rightarrow \sigma^*$ signals as a steep decrease in the absorption energies with respect to internuclear distance. The Na $2p \rightarrow \sigma^*$ transitions, on the other hand, do not induce charge transfer, and the potential character remains ionic. The potential minima are slightly shifted to shorter internuclear distance, from 2.7 Å to 2.5 Å,

after the core-to-valence probe excitation (Fig. 2). As such, the transition energy of the $2p \rightarrow \sigma^*$ signal around the Franck-Condon region exhibits an increasing trend in the transition energy with internuclear distance. Additional complexity is predicted to arise in a partially elongated region around $\sim$ 4 Å, namely, the Na absorption signals exhibit discontinuities and break up into multiple branches. This is a result of the avoided crossings that occur in the Na-2p core-excited states between the ionic and covalent potentials. The asymptotic part of the X(0^+) potential beyond the avoided crossing is of covalent character (Fig. 3(a)), which yields the lowest Na($^2S_{1/2}$) + I($^2P_{3/2}$) dissociation products. This dissociated state shows the sharp absorption lines associated with the I $4d \rightarrow 5p$ and Na $2p \rightarrow 3s$ transitions.

The excited A(0^+) state is of covalent character in the Franck-Condon region (Fig. 3(b)). This inner part of the potential is probed by the I $4d \rightarrow \sigma$ and Na $2p \rightarrow \sigma^*$ transitions, both of which are between covalent states (Fig. 2). The transition energies do not shift as dramatically as in the X(0^+) state toward the dissociation asymptote, which is consistent with the fact that the covalent potentials are flat (Fig. 2). The two other possible transitions, I $4d \rightarrow \sigma^*$ and Na $2p \rightarrow \sigma$, entail changes in the electronic character, but they hardly contribute to the absorption strengths because of the small spatial overlap between the valence and core orbitals. The asymptotic part of the A(0^+) potential, which is of ionic character, is probed only by the Na^+ $2p \rightarrow 3s$ transition.

C. Core-to-valence probe of predissociation

We simulated the core-level absorption spectra of the predissociation dynamics by combining the calculated core-to-valence absorption strengths with nonadiabatic nuclear wave-packet simulations. Plotted in Figs. 4(a-d) is the differential absorption (ΔA) computed from the UV-pump-on and UV-pump-off spectra, i.e., $\Delta A(\omega, t) = A_{\text{on}}(\omega, t) - A_{\text{off}}(\omega)$, in which ω is the photon energy and t is the probe time. The results are shown in Figs. 4(a,c) and 4(b,d) for the I-4d and Na-2p windows, respectively. In the arguments below, we focus on the strong absorption signals that originate from the bound wave-packet motion on the A(0^+) potential. The weaker signals originating from minor evolution pathways, including the diabatic return of the wave packet to the ionic X(0^+) potential, are analyzed in the Appendix.

The UV excitation at $t = 0$ triggers the charge transfer and promotes the molecule from the ionic X(0^+) state to the covalent A(0^+) state (Fig. 1). In the simulated absorption spectra shown in Figs. 4(a,b), the UV excitation induces a ground-state bleach ($\Delta A < 0$) in the Na-2p window, and excited-state absorption ($\Delta A > 0$) both in the I-4d and Na-2p windows. The ground-state bleach in the I-4d window, which corresponds to the $4d \rightarrow \sigma^*$ transitions, appears at 49.5 and 51.2 eV (not shown in Fig. 4(a)), and it does not overlap with the excited-state absorption, which corresponds to the $4d \rightarrow \sigma$ transitions.

The ground-state bleach signal (Figs. 4(b,d)) oscillates around 31.6 eV at the period of 133.3 fs. This is a direct signature of the vibrational wave packet launched in the ground X(0^+) state, and a brief analysis is as follows. In the simulated UV-excitation process, the excitation mechanism has mixed contributions from the resonance-enhanced Raman process and the internuclear-distance-dependent excitation (see Wei et al for details).[70] We assessed the phase of the oscillation in the center photon energy by following previous work;[70,71] least-squares fitting yielded a cosinusoidal oscillation with a phase of 0.31π, a value that falls between 0 (Raman) and $\pi/2$ (selective excitation). The natural ability to probe the dynamics in the ground electronic state is one of the advantages of the core-level absorption spectroscopy.

After the initial excitation, the photoexcited molecule smoothly evolves on the covalent A(0^+) potential. The early-time dynamics before the avoided crossing (0 to 150 fs) are well captured both in the I-4d and Na-2p windows (Figs. 4(a,b)). The I-$4d_{5/2}$ signal exhibits a slight but detectable peak shift from 45.9 to 46.1 eV (Fig. 4(a)). The monotonic energy variation enables one-to-one mapping of the absorption signals with respect to the internuclear distance.[72] This direct tracking of bond elongation exemplifies the sensitivity of core-level absorption to the structural information of molecules. The Na-2p signals exhibit more dramatic energy variations (Fig. 4(b)), but the interpretation is complicated due to the avoided crossings in the Na-2p core-excited potentials (Fig. 2).

When the photoexcited molecule reaches the avoided crossing at $\sim$ 190 fs, the majority of the wave packet proceeds adiabatically and transfers to the bound ionic potential (Fig. 1). In the core-level absorption spectra (Figs. 4(a,b)), the potential switching is characterized as a disappearance of the I-4d/Na-2p signals and appearance of the Na^+-2p signal. The strongest absorption peak in the Na-2p window exhibits a discontinuity and it jumps from 30.7 to 33.0 eV. Such a wide energy gap, however, cannot be explained by the variation in the potential energy alone. The discontinuity, instead, is attributed to the change in the electronic configuration from $[\sigma^1\pi^4\sigma^{*1}]$ to $[\sigma^2\pi^4\sigma^{*0}]$, and the core-level absorption imprints the electronic configurations on two distinguishable transitions, Na $2p \rightarrow \sigma$ and Na $2p \rightarrow \sigma^*$ (Fig. 3(b)). This result delineates the powerful capability of core-level absorption spectroscopy to directly probe the electronic dynamics at avoided crossings.

The long-term behavior of the absorption signals (-150 to 3400 fs) is shown in Figs. 4(c) and (d). It is clear that the periodic motion of the photoexcited wave packet on the predissociative potentials are directly characterized. Notably, the Na-2p/I-4d and Na^+-2p signals emerge out of phase, which intuitively signifies the covalent-ionic switching at the avoided crossing. We further analyzed the results by taking lineouts of the absorption signals at (1) 45.94 eV, (2) 45.65 eV, and (3) 33.08 eV, as highlighted by dashed lines in Figs. 4(c,d), and the results

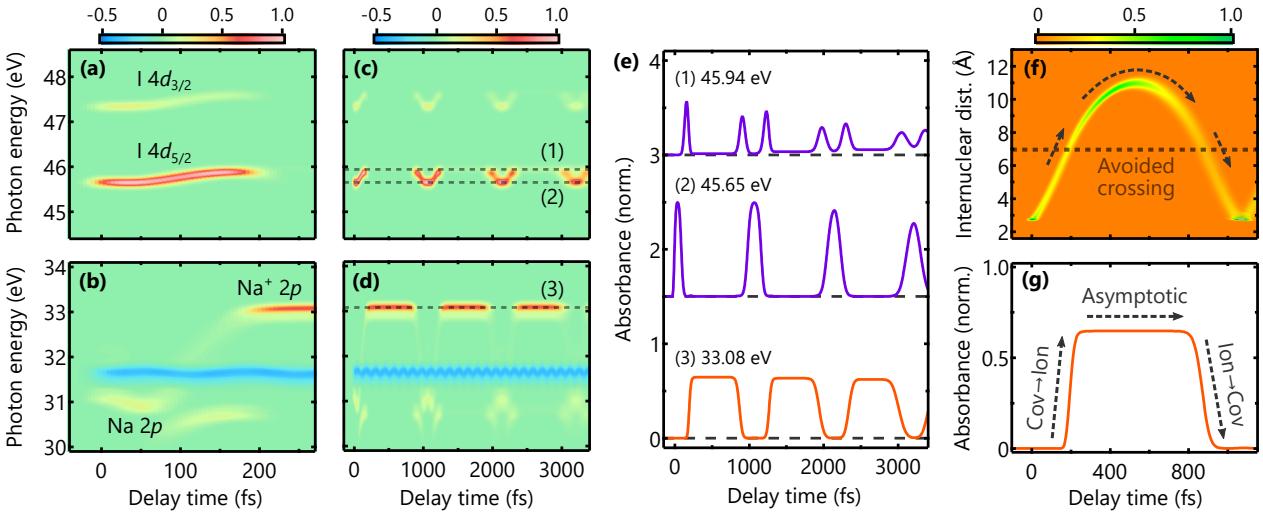

FIG. 4. **Simulated core-level absorption spectra of predissociation.** (a,b) Simulated differential absorption (ΔA) for the early-time (-45 fs to 270 fs) dynamics. (c,d) Results for the long-time (-150 fs to 3400 fs) dynamics. The periodic motion of the predissociation is clearly captured. (e) Absorption lineouts taken at (1) 45.94 eV, (2) 45.65 eV, and (3) 33.08 eV. Constant shifts are added to the plot for better visibility. (f) Simulated nuclear wave-packet motion ($|\psi(R,t)|^2$) on the adiabatic $A(0^+)$ potential. The dashed horizontal line indicates the location of the avoided crossing. (g) Detailed view of the absorption lineout at 33.08 eV, which corresponds to the Na^+ signal. The sharp rise and fall of the signal presents the direct evidence of electronic-character switching. The core-level absorption of Na^+ is insensitive to the nuclear wave-packet motion on the asymptotic part of the ionic potential.

are shown in Fig. 4(e).

The lineout (1) exhibits doublet features that resemble the off-resonant FTS signals characterized previously by Cong et al.[39] Thanks to the simultaneous probing of the entirety of the spectral features, the origin of the doublet structure is now apparent; the first doublet peak corresponds to the wave packet moving inward and the second doublet peak corresponds to the wave packet moving outward. Also, this lineout position corresponds to the I $^2P_{3/2} \rightarrow {}^2D_{5/2}$ atomic transition, and the periodic accumulation of the dissociation product is barely visible. The atomic signal from the dissociation product overlaps with the covalent molecular signals at the elongated internuclear distances, and they cannot be separated in absorption energy. The overlap problem is attributed to the natural broadening of the core-level absorption signals that is associated with the few-femtosecond autoionization lifetimes of the core-excited states. The stepwise accumulation of the dissociation product was more clearly characterized in the conventional FTS measurements[4,5] owing to the narrow spectral width of the Na D-line transitions (corresponding to a lifetime of 16.4 ns).[73]

The lineout (2) resembles the on-resonant FTS signals measured in the original work by Rose et al,[4] albeit with a different change in amplitude noted in the introduction. The latest experimental work confirmed that the on-resonant signal corresponds to probing the inner-turning point of the $A(0^+)$ potential,[50] and that is also the case in the present core-level absorption signals. The first peak appears at 41 fs, wherein the delay from zero is associated with the completion of the excitation by the 20-fs UV pulse. The second peak appears at 1070 fs, which compares well with the experimentally measured oscillation period at 320-nm excitation (1095 fs).[39] Overall, in the lineouts (1) and (2), the core-level absorption spectra can provide a large amount of information in one measurement, which would necessitate multiple measurements with variable probe wavelengths in the typical FTS experiments.

The lineout (3) corresponds to the Na^+ signal, or the wave packet in the asymptotic region of the ionic $A(0^+)$ potential, which has not been obtained in the conventional FTS experiments. We compared this signal with the simulated nuclear wave-packet motion to inspect the details, and the results are shown in Figs. 4(f,g). The sharp rise of the absorption signal at $\sim$ 190 fs reflects the first passage of the wave packet through the avoided crossing. The signal rise is completed in $\sim$ 55 fs, and during this time the center of the nuclear wave packet moves only from 6.3 Å to 7.8 Å (Fig. 4(f)). It is clear that at the avoided crossing this small variation in the nuclear coordinate can induce drastic switching of the electronic character. After the sharp rise, the absorption signal becomes completely invariant from 200 to 700 fs, even though the wave packet keeps evolving on the ionic potential extending out to 11.0 Å. The potential energy varies, between 7.0 Å and 11.0 Å, from 3.2 eV to 3.9 eV (Fig. 1), but this variation does not influence the core-level absorption signal. These results show that the core-level absorption is insensitive to the changes in the Coulomb interaction between the Na^+ and I^- ions, which constitutes the asymptotic part of the $A(0^+)$ po-

tential but does not modify the energy difference between the Na-2p and Na-3s orbitals.

The fact that core-level absorption is insensitive to the wave-packet motion on the ionic potential is beneficial in determining the dissociation probability. If we inspect the peak amplitude of the lineout (2) (Fig. 4(e)), which resembles the typical on-resonance FTS signal, it decreases by 8.1 % from 1070 fs to 2140 fs. This reduction is caused by the mixed contributions from the population decrease by the dissociation and the spatial broadening of the wave packet, as noted in the introduction. If we turn to the plateaus of the Na^+ signal (Fig. 4(e)), the amplitude decreases from the first plateau to the second plateau only by 1.8%. The probability of the diabatic passage across the avoided crossing in the current simulation is 0.9%, and taking into account that the wave packet meets the avoided crossing twice per every cycle, it is evident that the amplitude of the Na^+ signal represents a direct measure of the dissociation probability.

IV. CONCLUSIONS

We computed the valence and core-excited electronic structure of NaI by using the SO-GMC-QDPT method and simulated the core-level absorption spectra of the predissociation dynamics. Superb capabilities of the core-level absorption were highlighted, which include the continuous tracking of the wave-packet motion on the covalent potential and the direct characterization of the covalent-ionic switching at the avoided crossing. The method was found insensitive to the changes in the Coulomb interaction, which is the sole contribution to the asymptotic part of the ionic $A(0^+)$ potential. These results are in line with the interpretation that the core-level absorption is not simply probing the potential energies; instead, it is a direct probe of the valence orbital character and electronic configurations, the latter abruptly changing at the avoided crossing.[15] Overall, ultrafast XUV transient absorption spectroscopy will provide powerful and complementary windows into the predissociation dynamics, and we foresee its wider applications to molecular dynamics that involve elusive potential crossings.

APPENDIX: CONSIDERATION OF MINOR PATHWAYS

In the current simulations, the probability of the wave packet diabatically proceeding at the avoided crossing is 0.9% (Fig. 1). As such, absorption signals from the diabatic pathways, i.e., the dissociated atomic products from the wave packet that is moving outward and the vibrationally-excited ground-state molecule from the wave packet that is moving inward, are significantly weaker and not discussed, but present in the calculations. To visualize these weaker absorption signals, the simulated spectra for the I-4d window, the same data as in Figs. 4(a-d), are shown in Fig. 5 on a logarithmic scale. The absorption spectra in the Na-2p window are unsuitable to analyze the weaker signals due to the complex discontinuities caused by the avoided crossings in the core-excited potentials.

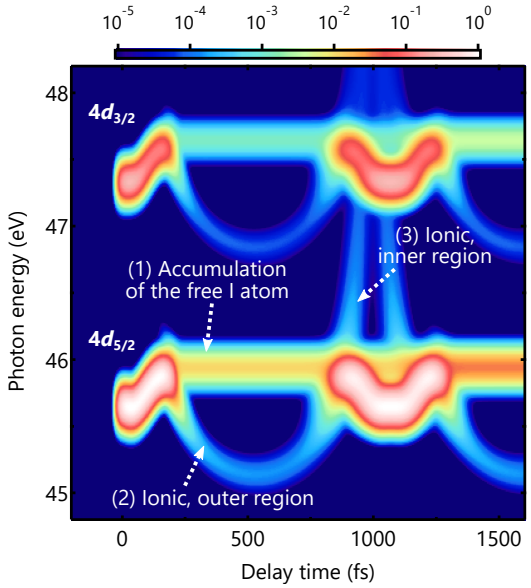

FIG. 5. **Simulated core-level absorption spectra shown on a logarithmic scale.** The same absorption data as in Figs. 4(a-d) are shown on a logarithmic scale to visualize the weaker signals. (1) The step-wise increment of the free I atom. (2) The wave-packet motion on the asymptotic part of the ionic $A(0^+)$ potential. (3) The wave packet on the inner region of the ionic $X(0^+)$ potential.

At $\sim$ 190 fs, the photoexcited molecule reaches the avoided crossing. In the diabatic pathway, the molecule will dissociate into the Na+I atoms, and the free I atom is characterized as a static absorption signal at 45.9 eV (Fig. 5, mark 1). Note that this feature is barely visible in the absorption lineout (1) shown in Fig. 4(e). From 45 eV to 46 eV, a sweeping peak shift is observed for the weak absorption signal (Fig. 5, mark 2), which originates from the wave-packet motion on the asymptotic part of the ionic $A(0^+)$ potential. In the main text, we argued that the ionic signal from the adiabatic pathway is only visible in the Na^+ window. However, strictly speaking, the I^- signal from the bound ionic state is not completely zero in the simulations, reflecting a tiny contribution of the covalent configuration to the ionic $A(0^+)$ potential.

At $\sim$ 870 fs, the wave packet on the ionic $A(0^+)$ potential returns to the avoided crossing, and the diabatic evolution here leads to the vibrationally excited molecule on the ionic $X(0^+)$ potential (Fig 1). The I-4d absorption signal captures this wave-packet motion in the photon energy from 46 eV to 47 eV (Fig. 5, mark 3). The signal corresponds to the $4d \rightarrow \sigma^*$ charge-transfer transition, and the large energy shift is an expected result from the analysis of Fig. 3(a). The wave packet reaches the inner-

turning point at 2.0 Å at $\sim$ 1000 fs and bounces back to the crossing region. Most of the wave packet adiabatically transfers the potentials from ionic to covalent and dissociates into the Na + I asymptote. The corresponding signal is not clearly captured due to the overlap with the other stronger signal (i.e., the wave packet on the covalent $A(0^+)$ potential).

ACKNOWLEDGMENTS

We acknowledge Prof. Klobukowski for answering our question about the basis sets. This work is supported by the US Army Research Office (ARO) (W911NF-14-1-0383) (Y.K., D.M.N., and S.R.L.) and the National Science Foundation (NSF) (CHE-1660417) (S.R.L. and equipment). T.Z. acknowledges the Natural Sciences and Engineering Research Council (NSERC) of Canada for research funding (RGPIN-2016-06276) and also York University for the start-up grant (481333). Y.K. also acknowledges financial support from the Funai Overseas Scholarship.

[1] C. V. Shank, Science **233**, 1276 (1986).
[2] A. H. Zewail, Science **242**, 1645 (1988).
[3] M. Dantus, M. J. Rosker, and A. H. Zewail, The Journal of Chemical Physics **87**, 2395 (1987).
[4] T. S. Rose, M. J. Rosker, and A. H. Zewail, The Journal of Chemical Physics **88**, 6672 (1988).
[5] T. S. Rose, M. J. Rosker, and A. H. Zewail, The Journal of Chemical Physics **91**, 7415 (1989).
[6] P. B. Corkum and F. Krausz, Nature Physics **3**, 381 (2007).
[7] F. Krausz and M. Ivanov, Rev. Mod. Phys. **81**, 163 (2009).
[8] S. R. Leone and D. M. Neumark, Faraday Discuss. **194**, 15 (2016).
[9] F. Calegari, A. Trabattoni, A. Palacios, D. Ayuso, M. C. Castrovilli, J. B. Greenwood, P. Decleva, F. Martín, and M. Nisoli, Journal of Physics B: Atomic, Molecular and Optical Physics **49**, 142001 (2016).
[10] K. Ramasesha, S. R. Leone, and D. M. Neumark, Annu. Rev. Phys. Chem. **67**, 41 (2016).
[11] H. J. Wörner, C. A. Arrell, N. Banerji, A. Cannizzo, M. Chergui, A. K. Das, P. Hamm, U. Keller, P. M. Kraus, E. Liberatore, P. Lopez-Tarifa, M. Lucchini, M. Meuwly, C. Milne, J.-E. Moser, U. Rothlisberger, G. Smolentsev, J. Teuscher, J. A. van Bokhoven, and O. Wenger, Structural Dynamics **4**, 061508 (2017).
[12] P. M. Kraus, M. Zürch, S. K. Cushing, D. M. Neumark, and S. R. Leone, Nature Reviews Chemistry **2**, 82 (2018).
[13] A. Bhattacherjee and S. R. Leone, Accounts of Chemical Research **51**, 3203 (2018).
[14] S. R. Leone, C. W. McCurdy, J. Burgdörfer, L. S. Cederbaum, Z. Chang, N. Dudovich, J. Feist, C. H. Greene, M. Ivanov, R. Kienberger, U. Keller, M. F. Kling, Z.-H. Loh, T. Pfeifer, A. N. Pfeiffer, R. Santra, K. Schafer, A. Stolow, U. Thumm, and M. J. J. Vrakking, Nature Photonics **8**, 162 (2014).
[15] Y. Kobayashi, K. F. Chang, T. Zeng, D. M. Neumark, and S. R. Leone, Science **365**, 79 (2019).
[16] G. A. Worth and L. S. Cederbaum, Annual Review of Physical Chemistry **55**, 127 (2004).
[17] B. G. Levine and T. J. Martínez, Annual Review of Physical Chemistry **58**, 613 (2007).
[18] S. Matsika and P. Krause, Annual Review of Physical Chemistry **62**, 621 (2011).
[19] W. Domcke and D. R. Yarkony, Annual Review of Physical Chemistry **63**, 325 (2012).
[20] M. S. Schuurman and A. Stolow, Annual Review of Physical Chemistry **69**, 427 (2018).
[21] B. J. Sussman, D. Townsend, M. Y. Ivanov, and A. Stolow, Science **314**, 278 (2006).
[22] S. Takeuchi, S. Ruhman, T. Tsuneda, M. Chiba, T. Taketsugu, and T. Tahara, Science **322**, 1073 (2008).
[23] T. Horio, T. Fuji, Y.-I. Suzuki, and T. Suzuki, Journal of the American Chemical Society **131**, 10392 (2009).
[24] D. Polli, P. Altoè, O. Weingart, K. M. Spillane, C. Manzoni, D. Brida, G. Tomasello, G. Orlandi, P. Kukura, R. A. Mathies, M. Garavelli, and G. Cerullo, Nature **467**, 440 (2010).
[25] H. J. Wörner, J. B. Bertrand, B. Fabre, J. Higuet, H. Ruf, A. Dubrouil, S. Patchkovskii, M. Spanner, Y. Mairesse, V. Blanchet, E. Mével, E. Constant, P. B. Corkum, and D. M. Villeneuve, Science **334**, 208 (2011).
[26] M. Kowalewski, K. Bennett, K. E. Dorfman, and S. Mukamel, Phys. Rev. Lett. **115**, 193003 (2015).
[27] T. Horio, R. Spesyvtsev, K. Nagashima, R. A. Ingle, Y.-i. Suzuki, and T. Suzuki, The Journal of Chemical Physics **145**, 044306 (2016).
[28] W. K. Peters, D. E. Couch, B. Mignolet, X. Shi, Q. L. Nguyen, R. C. Fortenberry, H. B. Schlegel, F. Remacle, H. C. Kapteyn, M. M. Murnane, and W. Li, Proceedings of the National Academy of Sciences **114**, E11072 (2017).
[29] M. C. E. Galbraith, S. Scheit, N. V. Golubev, G. Reitsma, N. Zhavoronkov, V. Despré, F. Lépine, A. I. Kuleff, M. J. J. Vrakking, O. Kornilov, H. Köppel, and J. Mikosch, Nature Communications **8**, 1018 (2017).
[30] A. von Conta, A. Tehlar, A. Schletter, Y. Arasaki, K. Takatsuka, and H. J. Wörner, Nature Communications **9**, 3162 (2018).
[31] A. E. Boguslavskiy, O. Schalk, N. Gador, W. J. Glover, T. Mori, T. Schultz, M. S. Schuurman, T. J. Martínez, and A. Stolow, The Journal of Chemical Physics **148**, 164302 (2018).
[32] J. Yang, X. Zhu, T. J. A. Wolf, Z. Li, J. P. F. Nunes, R. Coffee, J. P. Cryan, M. Gühr, K. Hegazy, T. F. Heinz, K. Jobe, R. Li, X. Shen, T. Veccione, S. Weathersby, K. J. Wilkin, C. Yoneda, Q. Zheng, T. J. Martinez, M. Centurion, and X. Wang, Science **361**, 64 (2018).
[33] T. J. A. Wolf, D. M. Sanchez, J. Yang, R. M. Parrish, J. P. F. Nunes, M. Centurion, R. Coffee, J. P. Cryan, M. Gühr, K. Hegazy, A. Kirrander, R. K. Li, J. Ruddock, X. Shen, T. Vecchione, S. P. Weathersby, P. M. Weber, K. Wilkin, H. Yong, Q. Zheng, X. J. Wang, M. P. Minitti, and T. J. Martínez, Nature Chemistry **11**, 504 (2019).
[34] M. E. Corrales, J. González-Vázquez, R. de Nalda, and L. Bañares, The Journal of Physical Chemistry Letters **10**, 138 (2019).
[35] V. Engel, H. Metiu, R. Almeida, R. Marcus, and A. H. Zewail, Chemical Physics Letters **152**, 1 (1988).
[36] J. Wang, A. Blake, D. McCoy, and L. Torop, Chemical Physics Letters **175**, 225 (1990).
[37] C. Meier, V. Engel, and J. S. Briggs, The Journal of Chemical Physics **95**, 7337 (1991).
[38] J. Herek, A. Materny, and A. Zewail, Chemical Physics Letters **228**, 15 (1994).
[39] P. Cong, G. Roberts, J. L. Herek, A. Mohktari, and A. H. Zewail, The Journal of Physical Chemistry **100**, 7832 (1996).
[40] M. Motzkus, S. Pedersen, and A. H. Zewail, The Journal of Physical Chemistry **100**, 5620 (1996).
[41] T. J. Martinez and R. D. Levine, The Journal of Chemical Physics **105**, 6334 (1996).
[42] T. J. Martinez and R. Levine, Chemical Physics Letters **259**, 252 (1996).
[43] C. Jouvet, S. Martrenchard, D. Solgadi, C. Dedonder-Lardeux, M. Mons, G. Grégoire, I. Dimicoli, F. Piuzzi, J. P. Visticot, J. M. Mestdagh, P. D'Oliveira, P. Meynadier, and M. Perdrix, The Journal of Physical Chemistry A **101**, 2555 (1997).
[44] E. Charron and A. Suzor-Weiner, The Journal of Chemical Physics **108**, 3922 (1998).
[45] K. B. Møller, N. E. Henriksen, and A. H. Zewail, The Journal of

Chemical Physics **113**, 10477 (2000).
[46]A. B. Alekseyev, H.-P. Liebermann, R. J. Buenker, N. Balakrishnan, H. R. Sadeghpour, S. T. Cornett, and M. J. Cavagnero, The Journal of Chemical Physics **113**, 1514 (2000).
[47]Y. Arasaki, K. Takatsuka, K. Wang, and V. McKoy, Phys. Rev. Lett. **90**, 248303 (2003).
[48]K. O. Korovin, E. Heinecke, A. Patzer, T. Liebig, O. S. Vasyutinskii, and D. Zimmermann, The European Physical Journal D **44**, 57 (2007).
[49]T. Leitner, F. Buchner, A. Luebcke, A. Rouzée, L. Rading, P. Johnsson, M. Odelius, H. O. Karlsson, M. Vrakking, and P. Wernet, EPJ Web of Conferences **41**, 02027 (2013).
[50]G. Rasskazov, M. Nairat, I. Magoulas, V. V. Lozovoy, P. Piecuch, and M. Dantus, Chemical Physics Letters **683**, 121 (2017).
[51]R. Geneaux, H. J. B. Marroux, A. Guggenmos, D. M. Neumark, and S. R. Leone, Philosophical Transactions of the Royal Society A **377**, 20170463 (2019).
[52]M. Chini, X. Wang, Y. Cheng, and Z. Chang, J. Phys. B **47**, 124009 (2014).
[53]R. S. Mulliken, Phys. Rev. **51**, 310 (1937).
[54]M. W. Schmidt, K. K. Baldridge, J. A. Boatz, S. T. Elbert, M. S. Gordon, J. H. Jensen, S. Koseki, N. Matsunaga, K. A. Nguyen, S. Su, T. L. Windus, M. Dupuis, and J. A. Montgomery, Journal of Computational Chemistry **14**, 1347 (1993).
[55]H. Nakano, R. Uchiyama, and K. Hirao, Journal of Computational Chemistry **23**, 1166 (2002).
[56]M. Miyajima, Y. Watanabe, and H. Nakano, The Journal of Chemical Physics **124**, 044101 (2006).
[57]R. Ebisuzaki, Y. Watanabe, and H. Nakano, Chemical Physics Letters **442**, 164 (2007).
[58]T. Zeng, The Journal of Chemical Physics **146**, 144103 (2017).
[59]Y. Kobayashi, T. Zeng, D. M. Neumark, and S. R. Leone, Structural Dynamics **6**, 014101 (2019).
[60]E. Miyoshi, Y. Sakai, K. Tanaka, and M. Masamura, Journal of Molecular Structure **451**, 73 (1998).
[61]M. Sekiya, T. Noro, Y. Osanai, and T. Koga, Theoretical Chemistry Accounts **106**, 297 (2001).
[62]J. R. Rusk and W. Gordy, Phys. Rev. **127**, 817 (1962).
[63]G. O'Sullivan, C. McGuinness, J. T. Costello, E. T. Kennedy, and B. Weinmann, Phys. Rev. A **53**, 3211 (1996).
[64]H. W. Wolff, K. Radler, B. Sonntag, and R. Haensel, Zeitschrift für Physik **257**, 353 (1972).
[65]J. Lindner, H. Bluhm, A. Fleisch, and E. Tiemann, Canadian Journal of Physics **72**, 1137 (1994).
[66]M. Monnerville and J. Robbe, The European Physical Journal D - Atomic, Molecular, Optical and Plasma Physics **5**, 381 (1999).
[67]D. T. Colbert and W. H. Miller, The Journal of Chemical Physics **96**, 1982 (1992).
[68]W. T. Pollard and R. A. Friesner, The Journal of Chemical Physics **100**, 5054 (1994).
[69]U. V. Riss and H. Meyer, The Journal of Chemical Physics **105**, 1409 (1996).
[70]Z. Wei, J. Li, L. Wang, S. T. See, M. H. Jhon, Y. Zhang, F. Shi, M. Yang, and Z.-H. Loh, Nature Communications **8**, 735 (2017).
[71]E. R. Hosler and S. R. Leone, Phys. Rev. A **88**, 023420 (2013).
[72]Z. Wei, L. Tian, J. Li, Y. Lu, M. Yang, and Z.-H. Loh, The Journal of Physical Chemistry Letters **9**, 5742 (2018).
[73]T. Erdmann, H. Figger, and H. Walther, Optics Communications **6**, 166 (1972).